Nanoscale

PAPER

View Article Online
View Journal | View Issue

Cite this: *Nanoscale*, 2020, **12**, 15175

Strong influence of strain gradient on lithium diffusion: flexo-diffusion effect†

Gao Xu,[a] Feng Hao,[b] Mouyi Weng,[c] Jiawang Hong,*[d] Feng Pan*[c] and Daining Fang*[a,e]

Received 14th May 2020,
Accepted 1st July 2020

DOI: 10.1039/d0nr03746j

rsc.li/nanoscale

Lithium ion batteries (LIBs) work under a sophisticated external force field and the electrochemical properties could be modulated by strain. Owing to electro-mechanical coupling, the change of micro local structures can greatly affect the lithium (Li) diffusion rate in solid state electrolytes and the electrode materials of LIBs. In this study, we found, through first-principles calculations, that the strain gradient in bilayer graphene (BLG) significantly affects the Li diffusion barrier, which is termed as the flexo-diffusion effect. The Li diffusion barrier substantially decreases/increases under a positive/negative strain gradient, leading to a change of Li diffusion coefficient of several orders of magnitude at 300 K. Interestingly, the regulation effect of strain gradient is much more significant than that of a uniform strain field, which can have a remarkable effect on the rate performance of batteries, with a considerable increase in the ionic conductivity and a slight change of the original material structure. Moreover, our *ab initio* molecular dynamics simulations (AIMD) show that the asymmetric distorted lattice structure provides a driving force for Li diffusion, resulting in oriented diffusion along the positive strain gradient direction. We predict the new phenomenon of a flexo-diffusion effect from a theoretical calculation aspect, these findings could extend present LIB technologies by introducing a novel strain gradient engineering.

1. Introduction

Lithium (Li) ion batteries (LIBs) with a high capacity and high rate have attracted tremendous attention. In order to increase the power density and charge/discharge efficiency of LIBs, it is imperative to improve the rate performance of electrode materials. From the fundamental physics point of view, it is essential to improve the electronic and ionic conductivities of the electrode materials.[1] Li-ion transport pathways and rates in LIBs have been widely studied by first-principles calculations, *e.g.*, the faster Li-ion diffusion *vs.* the larger layer distance in layered Li transition metal (TM) oxides $LiTMO_2$ (TM = Ni, Mn, Co, or $Ni_xMn_yCo_z$, $x + y + z = 1$) as cathode materials,[2] and high-throughput methods.[3] New transport mechanisms, such as cooperative transport and liquid-like transport enabling a fast Li-ion diffusion in solid electrolyte, were proposed,[4–6] and new materials were predicted under common conditions by focusing on the material itself.[7,8]

Previous successful strategies to improve the diffusion properties are mainly related to chemical doping and morphology modulation, such as nanosizing and carbon coating.[9,10] Besides, strain engineering is also an effective approach to modulate the LIB performance without changing the chemical constituents of the electrode materials. Strain has been shown as an effective method for tuning the electronic, transport, and optical properties of LIBs for decades.[11–16] In particular, the ionic conductivity of many electrode materials can be significantly enhanced by applying a uniform strain.[17–21] A previous study showed that the activation barrier is very sensitive to the Li concentration due to the strongly varying *c*-lattice parameter of the layered intercalation compounds,[22] the essential reason for that is the uniform strain in the *c*, *i.e.* out-of-plane, direction. With the rapid development of flexible electronics, LIBs have also been considered as key components in flexible, stretchable and wearable devices,[23–25] which inevitably involve a strain gradient. Therefore, in addition to strain, the strain gradient may introduce new regulative phenomena and efficiently regulative the effect on Li-ion diffusion in electrode materials. However, the strain gradient effect is rarely studied in LIBs.

[a]*State Key Laboratory for Turbulence and Complex Systems & Center for Applied Physics and Technology, College of Engineering, Peking University, Beijing 100871, P.R. China. E-mail: fangdn@bit.edu.cn*
[b]*Department of Engineering Mechanics, Shandong University, Jinan 250100, P.R. China*
[c]*School of Advanced Materials, Peking University, Shenzhen Graduate School, Shenzhen 518055, P.R. China. E-mail: panfeng@pkusz.edu.cn*
[d]*School of Aerospace Engineering, Beijing Institute of Technology, Beijing 100081, P.R. China. E-mail: hongjw@bit.edu.cn*
[e]*Institute of Advanced Structure Technology, Beijing Institute of Technology, Beijing 100081, P.R. China*

†Electronic supplementary information (ESI) available. See DOI: 10.1039/d0nr03746j

Interestingly, the strain gradient effect recently attracted tremendous attention in electro-mechanical materials,[26,27] termed as flexoelectricity, which reflects a novel coupling between an electric polarization and a strain gradient.[28,29] Flexoelectricity is a universal property allowed by symmetry in any dielectric materials and therefore significantly broadens the choice of materials for applications in electromechanical sensors and actuators. In addition, the magnitude of the strain gradient in nanostructures ($\sim 10^9$ m^{-1})[30,31] was found to be remarkably higher than that in bulk materials ($\sim 10^0$ m^{-1}),[32,33] indicating it may significantly affect the properties at nanoscale or even induce new phenomena.[34–36] However, a strain gradient has not been applied to modulate the diffusion properties in LIBs yet. Compared to the uniform strain modulation effect, the strain gradient may also provide a remarkable modulation effect or account for some novel phenomena for LIBs. For example, very recently, it was found that a giant strain gradient appears in deposited Li film on a Cu substrate, which may drive Li dendrite growth.[37] In this study, we will propose and demonstrate that the diffusion barrier, which dominates the ion conductivity, can be significantly modulated by strain gradient. Herein, the change of diffusion and its corresponding properties induced by strain gradient are termed as the flexo-diffusion effect.

To demonstrate this, we choose bilayer graphene (BLG) as prototype to explore the flexo-diffusion effect induced by a strain gradient. Graphene, the most well-studied two-dimensional (2D) material, exhibits a unique capacity in LIBs because of its high charge carrier mobility,[38] large surface area[39] and a broad electrochemical window.[40] Up to date, graphene-based materials have been utilized as electrode materials for batteries with great success.[41–45] However, the value of the Li diffusion barrier is 0.327 eV for graphene,[46] which is larger than that of other 2D materials, such as 0.25 eV on MoS_2 [47] and 0.08 eV on phosphorene.[48] Furthermore, Li diffusion in carbonaceous nanostructures is still not understood fully because of the lack of reliable experimental methods.[49] Therefore, it is essential to theoretically evaluate the diffusion barrier and path of Li.[50] Strain is particularly useful when engineering 2D crystals because these reduced-dimensional structures can sustain much larger strains than bulk crystals. Monolayer graphene was reported to be strained up to its intrinsic limit (~25%) without substantially damaging its crystal structures,[51] providing a dramatically wide range for tuning its mechanical and electronic performance. Recently, Chen *et al.*[52] reported that origami is an efficient way to convert graphene into atomically precise, complex nanostructures, which could controllably apply a strain gradient in graphene at the nanoscale. More importantly, as a representative 2D layered electrode material, the investigation of the flexo-diffusion effect of graphene can also provide a good reference for other 2D layered electrode materials and bulk crystals with inhomogenously distorted microstructures.

In this work, we investigate the strain gradient dependence of the Li diffusion barrier in BLG from a theoretical level by a first-principles method. We find that the flexo-diffusion effect strongly influences the Li diffusion in BLG. It shows that the Li diffusion barrier decreases/increases substantially under a positive/negative strain gradient, and the ionic conductivity increases by several orders of magnitude with a positive strain gradient at 300 K. Besides, the modulation of strain gradient is more efficient than that of uniform strain. Moreover, the asymmetric Li potential energy distribution induced by a strain gradient provides a driving force to drive Li oriented motion along the positive gradient direction, which cannot be realized in a uniform strain field. The flexo-diffusion effect provides a new approach to tune and optimize lithium diffusion in LIB applications.

2. Computational details

All the calculations are performed using the Vienna *ab initio* simulation package (VASP),[53,54] which is based on density functional theory (DFT). Projector-augmented-wave (PAW) potentials[55] are used to take into account the electron–ion interactions, while the electron exchange–correlation interactions are treated using the generalized gradient approximation (GGA)[56] in the scheme of Perdew–Burke–Ernzerhof. Taking into consideration the van der Waals forces, the results are calculated at the DFT-D2 level.[57] To analyze the Li diffusion in between layers of graphite, we simulate the Li diffusion in between two layers for BLG. The unit cell (8 carbon atoms) is obtained from an AB stacked hexagonal graphite; the two orthogonal in-plane lattice vectors are used for subsequent strain gradient applications. Atomic relaxation of the unit cell is performed with the energy and force convergence criterion of 1×10^{-6} eV and 0.001 eV $Å^{-1}$, respectively. A vacuum space of ~20 Å is placed between adjacent layers to avoid mirror interactions. A plane wave cutoff of 600 eV is set in our calculations with K-point sampling of $9 \times 12 \times 1$ grids. The carbon atom positions are fixed in other calculations. The diffusion barrier calculations and potential energy distribution calculations are performed on the $3 \times 2 \times 1$ and $4 \times 2 \times 1$ supercells, respectively. To simulate Li diffusion inside the BLG, we perform minimum energy path profiling using the climbing image nudged elastic band (CI-NEB) method as implemented in the VASP transition state tools,[58,59] where Li positions are relaxed. The calculated diffusion barriers are defined in ESI Note 1.† The kinetic properties of Li in different strain fields of BLG are studied using the *ab initio* molecular dynamics (AIMD) method. The simulations are performed on the $3 \times 2 \times 1$ supercell with only Γ point sampling in the Brillouin zone. We perform constant volume and temperature (NVT) AIMD calculations with a Nose thermostat[60] for 6000 steps with a time step of 1 fs, which is enough to indicate the motion trend of Li atoms.

3. Results and discussion

Our calculated interlayer spacing of BLG is 3.24 Å, which agrees well with other theoretical calculations (3.25 Å (ref. 61)

and 3.28 Å (ref. 62)) and is slightly smaller than experimental data for the lattice parameter $c/2$ of bulk graphite (3.35 Å (ref. 63)). The pristine interlayer spacing of BLG is set to 3.24 Å, *i.e.* no applied strain. To analyze Li diffusion properties in BLG, the Li adsorption positions should be first verified. Fig. 1a shows the local configuration of BLG. We follow a previous study[64] and consider two sites with high symmetry: the site on the top of a carbon atom (TT) and the site in the center of a hexagon (HT). For the stage-I compound LiC_6 of graphite, the HT is the most stable adsorption site.[64] To simulate the Li diffusion in between two layers of BLG, two high symmetrical paths of Li diffusion are considered, including HT–TT and HT–HT, as shown in Fig. 1a. The results in Fig. 1b and c show that the path HT–HT has a length of 1.47 Å, with a much lower energy barrier (287 meV) than that of the HT–TT diffusion path. Thus, the process of Li diffusion in BLG is repeated from one HT position to its adjacent HT position.

To analyze the strain modulation effect on Li diffusion inside BLG, we explore Li diffusion inside the BLG in different strain fields. All the applied strains are in the out-of-plane direction. Fig. 2 shows the schematic calculation configuration. Here, all the intercalated Li atoms are located in the left part of the supercell, as shown in Fig. 2a. The adsorption sites of Li labeled A to D in Fig. 2a are the main adsorption positions in the following calculations. We construct a supercell with a periodic strain to induce a strain gradient without breaking the periodic boundary condition for DFT calculations,[65] as shown in Fig. 2c and d. In this supercell, the bottom graphene layer keeps flat while the interlayer spacing $d(x)$ linearly changes following $d(x) = d_0 \times (1 + \eta x)$ until the middle of the supercell ($x = L/2$, L is the length of supercell in the x direction), where d_0 is the interlayer spacing of pristine BLG (3.24 Å) and η is the constant applied strain gradient; then, the interlayer spacing reversely changes from the middle to the end in the direction. The magnitude of strain in the middle of the x-lattice of the supercell is defined as the mid-strain ε_m ($\varepsilon_m = \eta L/2$), which can be used to represent the strain gradient in an alternative way. Mid-strain is the maximum/minimum strain in the BLG with a strain gradient. We adopt mid-strain ε_m to compare with the uniform strain cases in which the strain magnitude is the same as ε_m. In this way, the difference between the strain gradient case and the uniform strain case will come from the strain gradient effect. We also define the positive strain gradient as $\eta > 0$ ($\varepsilon_m > 0$) and negative strain gradient as $\eta < 0$ ($\varepsilon_m < 0$), as shown in Fig. 2c and d.

Then, we first consider the effect of a uniform strain on Li diffusion in BLG. Uniaxial stress is applied in the out-of-plane direction. The energy profiles for the Li pathways are calculated in four cases: pristine (0%), ±10% and 20% strain. In Fig. 3a, we can see that the Li diffusion barrier increases under compressive strain while it decreases under tensile strain. As the strain changes from −10% to 20%, the energy barrier drops from 0.61 eV to 0.14 eV, which indicates that the Li diffusion coefficient becomes larger/smaller with the interlayer spacing of BLG elongated/compressed. Similar results were also found for interlayer Li diffusion barriers in stage-II compounds in a previous work.[17] It can be easy to understand this tuning effect of the Li diffusion barrier for a layered structure by an external out-of-plane strain. When the distance of two graphene layers increases/decreases under an applied strain, the bonding effect between the diffusion Li atom and its adjacent carbon atoms becomes weaker/stronger, and thus the diffusion transition energy, *i.e.* energy barrier, decreases/increases. In fact, this phenomenon was also verified in other layered electrode materials from first-principles calculations for uniform strain modulation.[18–20] Hao *et al.* summarized that the activation energy (diffusion barrier) of Li diffusion can be approximately expressed by a linear relationship with strain[66]

$$E_B = A_0 + A_1\varepsilon \quad (1)$$

where A_0 and A_1 are material parameters. In this study, ε is considered as the strain in the out-of-plane direction for layered materials in LIBs. Based on the above discussion, A_1 should be negative, representing the modulation effect on Li diffusion by a uniform strain. A_0 indicates the intrinsic Li diffusion barrier of materials.

Next, we explore the flexo-diffusion effect induced by a strain gradient. To compare the effects of uniform strain and a strain gradient on diffusion, we calculate the energy barrier (from site A to site B) under various applied uniform strains

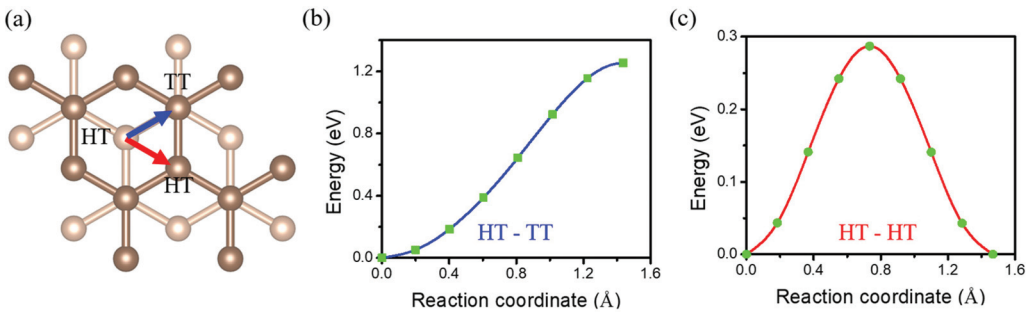

Fig. 1 (a) Schematic illustration for two possible diffusion paths in BLG. Dark brown and light brown represent the top and bottom carbon atomic layers, respectively. The HT and TT indicate two symmetry Li adsorption sites between BLG. The energy profiles for (b) path HT-TT and (c) path HT-HT.

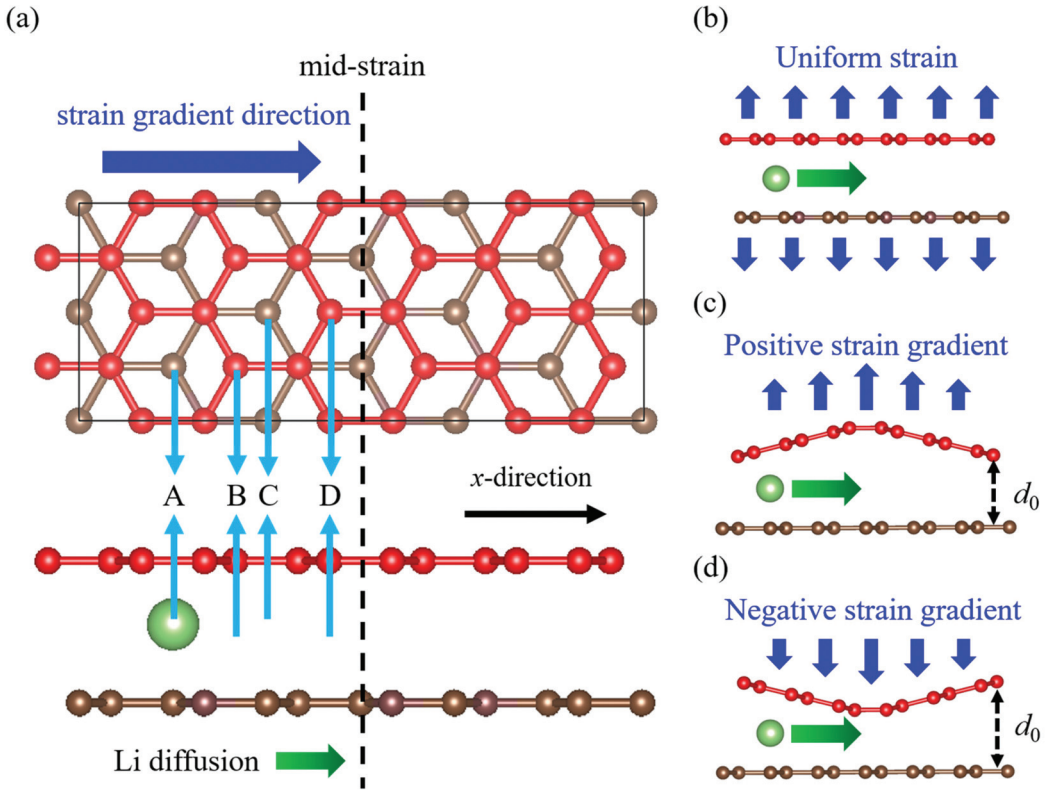

Fig. 2 (a) The top and side views of the pristine 3 × 2 × 1 supercell. The positions labeled A to D are the four stable HT sites for intercalated Li atoms. The schematic configurations from the side view for Li diffusion inside BLG: (b) uniform strain field, (c) positive strain gradient field, and (d) negative strain gradient field. In the case of a visible applied strain gradient, the crystal configuration is in the strain gradient field in this figure and the following figures are schematic configurations. The red and brown represent the top and bottom graphene layers, and the black frame indicates the supercell.

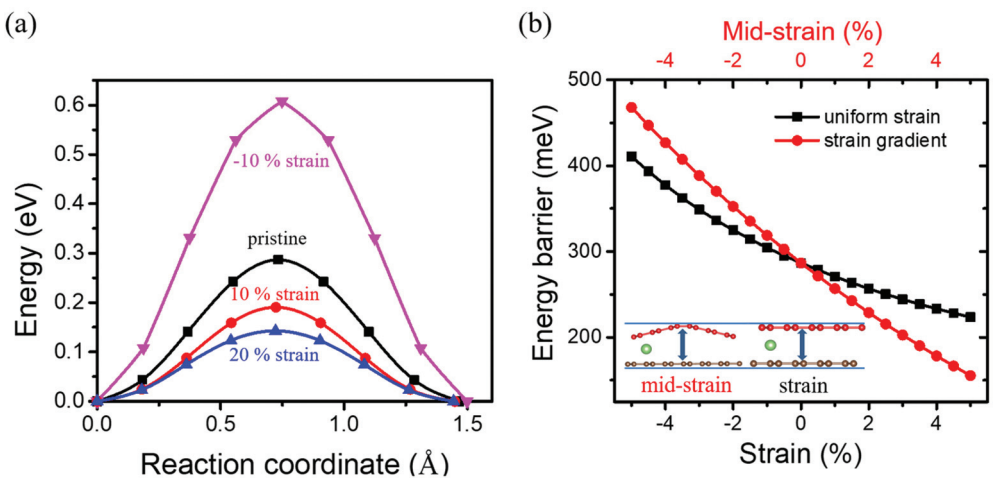

Fig. 3 (a) The energy profiles for Li pathways in four cases with uniform strain: pristine (0%), ±10% and 20%. (b) The variation of energy barrier of graphene as a function of uniform strain or mid-strain in a strain gradient field. All the diffusion paths in the calculations are from site A to site B.

and strain gradients, as shown in Fig. 3b, and the corresponding *x*-axis is aligning according to the schematic configurations in it. The energy barrier significantly decreases/increases when a positive/negative strain gradient is applied. This trend is the same as the case of uniform strain, because the magnitude of strain in the positive/negative strain gradient field is also positive/negative. However, it is worth noting that the calculated diffusion barriers in strain gradient fields are

near the x = 0 position of the supercell, where the magnitude of the strain is much smaller than that of corresponding uniform strain case. Nevertheless, we can still explicitly find that the energy barrier variation of strain gradient is larger than that of uniform strain in Fig. 3b. In addition, the diffusion barrier for the 5% mid-strain case of strain gradient (155 meV) is almost the same as that of the 20% uniform strain case (143 meV), which indicates that the strain gradient is much more efficient than the uniform strain to tune the diffusion barrier. Meanwhile, the lattice distortion is much smaller in the 5% mid-strain gradient case than that of the 20% uniform strain case, indicating the strain gradient can tune the barrier energy more efficiently than uniform strain with little lattice distortion, which is beneficial to the LIB applications.

The temperature-dependent transition rate can be evaluated by the Arrhenius equation, from which the diffusion constant (D) of Li follows[67]

$$D = D_0 \exp\left(\frac{-E_B}{k_B T}\right) \quad (2)$$

where D_0 is the proportionality coefficient, E_B is the activation energy, k_B is Boltzmann's constant and T is the absolute temperature set to 300 K. According to eqn (2), the diffusion mobility of Li along the positive strain gradient direction of a 5% mid-strain is about 1.6×10^2 times faster than that of pristine BLG at room temperature, the corresponding magnitude of strain gradient is about 8×10^7 m^{-1} (comparable to the strain gradient in other nanostructures[30,31]). In general, effectively tuning Li diffusion mobility usually requires a large strain, which is difficult to apply and it may also induce material structure failure or even damage. Here, we find that a strain gradient induced by a small magnitude strain can modulate the diffusion properties, which is much more effective than a uniform strain. The results suggest that a lattice strain gradient can have a remarkable and efficient effect on the rate performance of batteries, with a significant increase in the ionic conductivity but only a slight change of the material structure at the nanoscale. Therefore, an extremely high-rate capability and high-efficiency modulation are expected for strain gradient modulated graphene-based or other 2D material-based LIBs. On the other hand, for the -8×10^7 m^{-1} negative strain gradient case (−5% mid-strain), the diffusion mobility of Li is ~10^{-5} times smaller than that of pristine Li, indicating an extremely strong inhibition effect on Li diffusion. The negative strain gradient offers a significant suppression effect on diffusion, which suggests that this situation should be avoided in the flexible electronic devices in order to make LIBs work effectively. Besides, the huge distinction between positive/negative strain gradient effects on diffusion may introduce novel structural design, such as a switch based on a force sensor, to layered solid electrolytes, layered electrode materials and even all-solid-state batteries.

In order to study the mechanisms of the flexo-diffusion effect and the reason for the difference in modulation effect between uniform strain and strain gradient, we calculate the potential energy profiles of Li in BLG along the diffusion path with five unit-paths, as shown in Fig. 4a. Three conditions are considered for the strain fields: pristine, 5% uniform strain and strain gradient with 5% mid-strain. Generally, the Li diffusion barrier is determined by the potential energy surface along the diffusion pathway, which is related to both the crystalline structure and the local atomic species of the compound. When the strain field is uniform (including pristine BLG), the Li atom experiences a periodic potential field established by the layered carbon framework, and thus the energy variation in the diffusion path is also periodic. When a positive strain gradient is introduced, the symmetry of the lattice is broken, and the Li potential energies of two adjacent stable positions are changed, as shown in Fig. 4b. Due to the lower Li potential energy at the site with a larger strain, the asymmetry decreases the Li potential energy in the whole diffusion path. As a result, the peak of the Li potential energy of each unit path, *i.e.* diffusion barrier, in the diffusion path significantly decreases, thereby increasing the conductivity. In contrast,

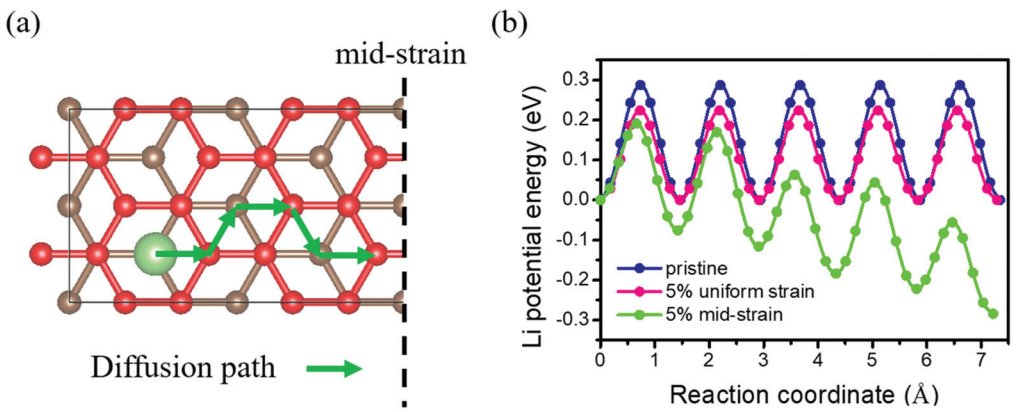

Fig. 4 (a) The left half part of 4 × 2 × 1 supercell and the calculation diffusion unit-paths hopping between adjacent HT sites. The red and brown represent the top and bottom carbon atomic layers, respectively. (b) The energy profiles of the Li atom along the diffusion path in different strain fields. The magnitude of the strain gradient for the strain gradient configuration is about 3×10^7 m^{-1}.

when the Li atom diffuses along the negative strain gradient direction, the next stable position is under a lower strain and with a higher potential energy, and thus the energy barrier will increase. This is explicitly shown in the green curve in Fig. 4b from the right to the left, which indicates the negative strain gradient case. Our results demonstrate that the flexo-diffusion effect originates from the symmetry breaking of the potential energy field in a crystal lattice due to the strain gradient.

To further explore the flexo-diffusion effect, we calculate energy barriers with an additional uniform strain or diffusion path deviating from the x direction. Firstly, to study the modulation effect of a uniform strain on BLG already in a strain gradient field, we apply an additional uniform strain ε to the strain gradient case, *i.e.* the interlayer spacing following $d(x) = d_0 \times (1 + \varepsilon + \eta_0 x)$. Fig. 5a shows the change of barrier with the additional uniform strain based on ±5% mid-strain configurations. It is observed that the linear strain modulation effect is also satisfied for strain gradient structures. Based on the results in Fig. 3b and 5a, the strain gradient effect could also be assumed as a linear effect, a superposition on the original strain effect. The influence of additional uniform strain on the −5% mid-strain case is more obvious than that of the 5% mid-strain case, due to the larger magnitude of the energy barrier under negative strain. Secondly, it is expected that the Li diffusion deviating from the strain gradient direction (x direction, deviating angle is θ) will also affect the energy barrier. The energy barriers of path-2 (from site B to site C in Fig. 2a, $\theta = 60°$) under different strain fields are calculated, and are compared with that of path-1 (from site A to site B in Fig. 2a, $\theta = 0$), as shown in Fig. 5b. The flexo-diffusion effect for path-2 with $\theta = 60°$ is significantly weaker than that of path-1 with $\theta = 0$. This shows that the flexo-diffusion effect also depends on the deviating angle between the unit diffusion direction and the strain gradient direction, in which the flexo-diffusion effect achieves a maximum when $\theta = 0$ (enhancement for a positive strain gradient) or $\theta = 180°$ (resistance for a negative strain gradient). Therefore, there should be an angle correction $f(\theta)$ included in the relationship between the energy barrier and the strain gradient. Then, the Li diffusion energy barrier in layered compounds for a certain configuration can be given as in eqn (3) which is further extended from eqn (1) by introducing the flexo-diffusion effect:

$$E_B = A_0 + A_1\varepsilon + A_2 \frac{d\varepsilon}{dx} f(\theta) \quad (3)$$

where A_0 is the intrinsic Li diffusion barrier, A_1 is the response of the energy barrier to the uniform strain, A_2 is the response of the energy barrier to the strain gradient, and $\frac{d\varepsilon}{dx}$ is the strain gradient in the x direction. Based on our results and discussion, the parameter A_2 should also be negative. Though we do not know the exact function form of $f(\theta)$, we can take its value to 1 for the case of $\theta = 0$ for studying the diffusion properties along the strain gradient direction. It will be beneficial to obtain the value of material parameters A_0, A_1 and A_2 for an accurate regulated response of strain for practical applications. From our DFT results, it is easy to fit the material parameters A_0, A_1 and A_2 for the case of $\theta = 0$, as $A_0 = 0.29$ eV, $A_1 = -1.7$ eV and $A_2 = -1.9 \times 10^{-9}$ eV m. For most layered electrode materials and various diffusion atoms, these three parameters can also be calculated with similar DFT calculations, which will be of importance for the strain engineering and material genetic engineering in batteries.

The strain and strain gradient can tune the diffusion barrier, which can help to design effective LIBs with mechanical strain. Because of the negative A_1, tensile strain can reduce the diffusion barrier, leading to an increase in conductivity. Nevertheless, applying tensile strain in the out-of-plane direction of the materials of LIBs may be a challenge in applications. Instead, a compressive strain is a better choice for applications. However, compressive strain increases the diffusion barrier and causes the reduction of the conductivity, which is harmful for the LIBs. Thanks to the flexo-diffusion effect, the conductivity can be still enhanced with a concen-

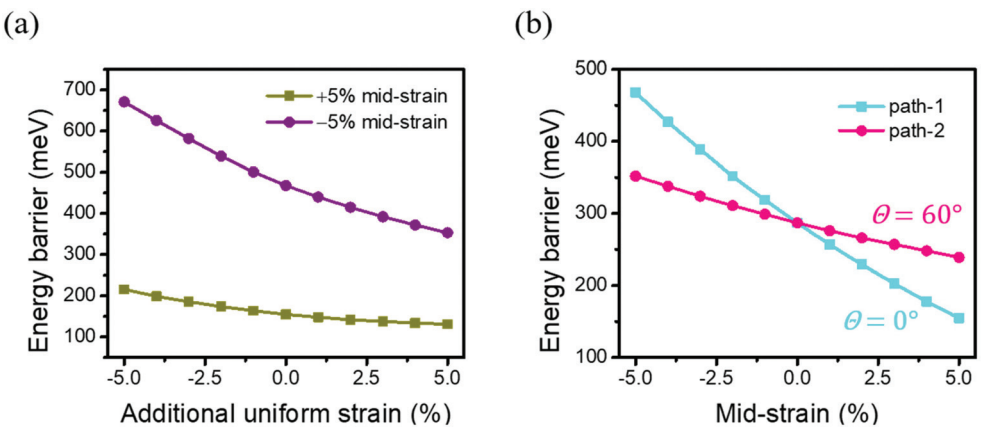

Fig. 5 (a) The change of energy barrier under the combination of a uniform strain and a strain gradient. The diffusion path is from site A to site B. The corresponding magnitude of the strain gradient is about $\pm 8 \times 10^7$ m^{-1} for the ±5% mid-strain cases. (b) The effect of diffusion angle on the energy barrier; path-1 is from site A to site B ($\theta = 0$) and path-2 is from site B to site C ($\theta = 60°$), sites A, B and C are shown in Fig. 2.

trated compressive stress, which can induce a positive strain gradient. The reason is that the enhancement of the positive strain gradient to the conductivity overcomes the reduction effect of the compressive strain. Therefore, a concentrated compressive stress, which is applicable in applications, could enhance the performance of LIBs by the flexo-diffusion effect. A detailed discussion can be found in ESI Note 2.†

It is noted that the gradient of some physical fields could drive oriented motions, such as thermal gradients on graphene to drive nanoflake motion,[68] chemical gradients on graphene to drive droplet motion[69] and proton-gradient-driven oriented motion of nanodiamonds grafted to graphene.[70] Thus, we also examine the motion trend of a Li atom inside BLG in different strain fields by AIMD at 500 K. Fig. 6 shows the displacement change of the Li atom from initial site with time in different strain fields: pristine (0%), 3%, 5% and 7% mid-strain. The displacement is defined as

$$d = \sqrt{(x - x_0)^2 + (y - y_0)^2 + (z - z_0)^2} \quad (4)$$

where (x_0, y_0, z_0) and (x, y, z) are the initial and current Li coordinates, respectively. When the strain gradient is zero or small, the Li atom only has a thermal motion around the initial stable site A. However, as the magnitude of the strain gradient increases, the Li atom will gradually move away from the initial site A. Interestingly, the simulated motion direction is exactly along the diffusion path discussed in the previous sections. For the case of a 5% mid-strain, the simulated motion result is from site A to site B, and the Li atom cannot keep moving to site C due to the deviation from the strain gradient direction, which has a higher energy barrier and requires a larger strain gradient to overcome. For the case of a 7% mid-strain, given that the energy barrier of the path from site B to site C further deceases, the Li atom can gradually move from site A to site B to site C to site D. The reason why Li atom moves back to site A in around 2 ps is due to thermal perturbation; the magnitude of stain gradient is large enough for the perturbation to make the Li atom randomly move back to site A. So far, we can theoretically conclude that the strain gradient can drive the oriented motion of Li atoms inside the BLG. The orientation contains two aspects: a positive strain gradient direction and along the diffusion path. Moreover, the motion speed could be tuned by the magnitude of the strain gradient. Such tunability and phenomenon in graphene provide additional capabilities in device design for applications, such as the self-charging technique and in electromechanical sensors and actuators.

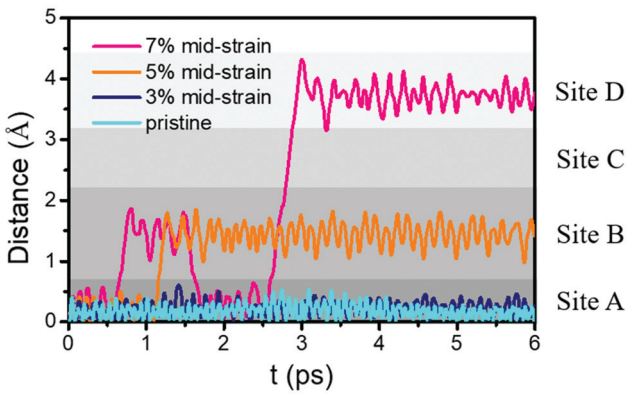

Fig. 6 The change of displacement and position of the Li atom inside BLG with time under different strain fields simulated by AIMD at 500 K. Each interval (presented in different shades of gray) indicates the range of the corresponding site position.

4. Conclusions

We propose a flexo-diffusion effect and investigate the diffusion properties of a Li atom inside BLG with a uniform strain and gradient strain fields from DFT calculations. It is found that the Li diffusion barrier in BLG is very sensitive to the strain gradient applied to the lattice, which is termed as a flexo-diffusion effect. The Li diffusion barrier decreases/increases substantially upon the positive/negative strain gradient being applied along the in-plane direction, leading to a change of the Li diffusion coefficient by several orders of magnitude at 300 K. Moreover, the effect of regulation of the strain gradient is more significant than that of a uniform strain field. We also investigate the Li potential energy distribution in BLG in different strain fields, which shows that the novel effect induced by the strain gradient is attributed to the asymmetric potential energy distribution for the Li diffusion. The asymmetric lattice structure also provides a driving force for the oriented motions of Li atoms, and the motion speed could be tuned by the magnitude of the strain gradient. Furthermore, graphene is used as a typical 2D layered electrode material, and we expect that the flexo-diffusion effect could also be applicable to other layered materials where Li atoms store and diffuse between interlayers. The flexo-diffusion effect may extend present LIB technologies by introducing the novel strain gradient engineering.

Conflicts of interest

There are no conflicts to declare.

Acknowledgements

The authors acknowledge support by the National Key Research and Development Program of China (No. 2016YFB0700600), and the Foundation for Innovative Research Groups of the National Natural Science Foundation of China (No. 11521202 and 11572040).

References

1 C. Y. Ouyang and L. Q. Chen, Physics towards next generation Li secondary batteries materials: A short review from

computational materials design perspective, *Sci. China: Phys., Mech. Astron.*, 2013, **56**, 2278–2292.

2 Y. Wei, J. Zheng, S. Cui, X. Song, Y. Su, W. Deng, Z. Wu, X. Wang, W. Wang, M. Rao, Y. Lin, C. Wang, K. Amine and F. Pan, Kinetics Tuning of Li-Ion Diffusion in Layered $Li(Ni_xMn_yCo_z)O_2$, *J. Am. Chem. Soc.*, 2015, **137**, 8364–8367.

3 D. Chen, J. Jie, M. Weng, S. Li, D. Chen, F. Pan and L. W. Wang, High throughput identification of Li ion diffusion pathways in typical solid state electrolytes and electrode materials by BV-Ewald method, *J. Mater. Chem. A*, 2019, **7**, 1300–1306.

4 B. Zhang, L. Yang, L. W. Wang and F. Pan, Cooperative transport enabling fast Li-ion diffusion in Thio-LISICON Li10SiP2S12 solid electrolyte, *Nano Energy*, 2019, **62**, 844–852.

5 A. Marcolongo and N. Marzari, Ionic correlations and failure of Nernst-Einstein relation in solid-state electrolytes, *Phys. Rev. Mater.*, 2017, **1**, 1–4.

6 K. Zhang, B. Zhang, M. Weng, J. Zheng, S. Li and F. Pan, Lithium ion diffusion mechanism in covalent organic framework based solid state electrolyte, *Phys. Chem. Chem. Phys.*, 2019, **21**, 9883–9888.

7 A. M. Nolan, Y. Zhu, X. He, Q. Bai and Y. Mo, Computation-accelerated design of materials and interfaces for all-solid-state lithium-ion batteries, *Joule*, 2018, **2**, 2016–2046.

8 Y. Wang, W. D. Richards, S. P. Ong, L. J. Miara, J. C. Kim, Y. Mo and G. Ceder, Design principles for solid-state lithium superionic conductors, *Nat. Mater.*, 2015, **14**, 1026–1031.

9 C. Delacourta, P. Poizota, S. Levasseurb and C. Masquelier, Size effect of carbon-free LiFePO4 powders: the key for superior energy density, *Electrochem. Solid-State Lett.*, 2006, **9**, A352–A355.

10 H. Huang, S. C. Yin and L. F. Nazar, Approaching theoretical capacity of LiFePO4 at room temperature at high rates, *Electrochem. Solid-State Lett.*, 2001, **4**, A170–A172.

11 K. Lai, M. Nakamura, W. Kundhikanjana, M. Kawasaki, Y. Tokura, M. A. Kelly and Z. X. Shen, Mesoscopic percolating resistance network in a strained manganite thin film, *Science*, 2010, **329**, 190–193.

12 M. R. Falvo, G. J. Clary, R. M. Taylor II, V. Chi, F. P. Brooks Jr., S. Washburn and R. Superfine, Bending and buckling of carbon nanotubes under large strain, *Nature*, 1997, **389**, 582–584.

13 J. H. Haeni, P. Irvin, W. Chang, R. Uecker, P. Reiche, Y. L. Li, S. Choudhury, W. Tian, M. E. Hawley, B. Craigo, A. K. Tagantsev, X. Q. Pan, S. K. Streiffer, L. Q. Chen, S. W. Kirchoefer, J. Levy and D. G. Schlom, Room-temperature ferroelectricity in strained $SrTiO_3$, *Nature*, 2004, **430**, 758–761.

14 R. S. Jacobsen, K. N. Andersen, P. I. Borel, J. Fage-Pedersen, L. H. Frandsen, O. Hansen, M. Kristensen, A. V. Lavrinenko, G. Moulin, H. Ou, C. Peucheret, B. Zsigri and A. Bjarklev, Strained silicon as a new electro-optic material, *Nature*, 2006, **441**, 199–202.

15 V. M. Pereira and A. H. C. Neto, Strain engineering of graphene's electronic structure, *Phys. Rev. Lett.*, 2009, **103**, 046801.

16 H. J. Conley, B. Wang, J. I. Ziegler, R. F. Haglund Jr., S. T. Pantelides and K. I. Bolotin, Bandgap Engineering of Strained Monolayer and Bilayer MoS_2, *Nano Lett.*, 2013, **13**, 3626–3630.

17 K. Persson, Y. Hinuma, Y. S. Meng, A. van der Ven and G. Ceder, Thermodynamic and kinetic properties of the Li-graphite system from first-principles calculations, *Phys. Rev. B: Condens. Matter Mater. Phys.*, 2010, **82**, 125416.

18 C. Tealdi, J. Heath and M. S. Islam, Feeling the strain: enhancing ionic transport in olivine phosphate cathodes for Li-and Na-ion batteries through strain effects, *J. Mater. Chem. A*, 2016, **4**, 6998–7004.

19 F. Ning, S. Li, B. Xu and C. Ouyang, Strain tuned Li diffusion in $LiCoO_2$ material for Li ion batteries: A first principles study, *Solid State Ionics*, 2014, **263**, 46–48.

20 J. Lee, S. J. Pennycook and S. T. Pantelides, Simultaneous enhancement of electronic and Li^+ ion conductivity in $LiFePO_4$, *Appl. Phys. Lett.*, 2012, **101**, 033901.

21 G. Xu, Y. Liu, J. Hong and D. Fang, Lithium intercalation drives mechanical properties deterioration in bulk and single-layered black phosphorus: A first-principles study, *2D Mater.*, 2020, **7**, 025028.

22 A. van der Ven and G. Ceder, Lithium diffusion mechanisms in layered intercalation compounds, *J. Power Sources*, 2001, **97**, 529–531.

23 F. Bonaccorso, Z. Sun, T. Hasan and A. C. Ferrari, Graphene photonics and optoelectronics, *Nat. Photonics*, 2010, **4**, 611.

24 J. H. Ahn and B. H. Hong, Graphene for displays that bend, *Nat. Nanotechnol.*, 2014, **9**, 737.

25 S. Bae, H. Kim, Y. Lee, X. Xu, J. S. Park, Y. Zheng, J. Balakrishnan, T. Lei, H. R. Kim, Y. I. Song, Y. J. Kim, K. S. Kim, B. Özyilmaz, J. H. Ahn, B. H. Hong and S. Iijima, Roll-to-roll production of 30-inch graphene films for transparent electrodes, *Nat. Nanotechnol.*, 2010, **5**, 574.

26 B. Wang, Y. Gu, S. Zhang and L. Q. Chen, Flexoelectricity in solids: Progress, challenges, and perspectives, *Prog. Mater. Sci.*, 2019, **106**, 100570.

27 P. Zubko, G. Catalan and A. K. Tagantsev, Flexoelectric effect in solids, *Annu. Rev. Mater. Res.*, 2013, **43**, 387–421.

28 J. Hong and D. Vanderbilt, First-principles theory of frozen-ion flexoelectricity, *Phys. Rev. B: Condens. Matter Mater. Phys.*, 2011, **84**, 180101.

29 J. Hong and D. Vanderbilt, First-principles theory and calculation of flexoelectricity, *Phys. Rev. B: Condens. Matter Mater. Phys.*, 2013, **88**, 174107.

30 Y. L. Tang, Y. L. Zhu, X. L. Ma, A. Y. Borisevich, A. N. Morozovska, E. A. Eliseev, W. Y. Wang, Y. J. Wang, Y. B. Xu, Z. D. Zhang and S. J. Pennycook, Observation of a periodic array of flux-closure quadrants in strained ferroelectric $PbTiO_3$ films, *Science*, 2015, **348**, 547–551.

31 P. Gao, S. Yang, R. Ishikawa, N. Li, B. Feng, A. Kumamoto, N. Shibata, P. Yu and Y. Ikuhara, Atomic-Scale

Measurement of Flexoelectric Polarization at $SrTiO_3$. Dislocations, *Phys. Rev. Lett.*, 2018, **120**, 267601.
32 P. Zubko, G. Catalan, A. Buckley, P. R. L. Welche and J. F. Scott, Strain-Gradient-Induced Polarization in $SrTiO_3$ Single Crystals, *Phys. Rev. Lett.*, 2007, **99**, 167601.
33 F. Zhang, P. Lv, Y. Zhang, S. Huang, C. M. Wong, H. M. Yau, X. Chen, Z. Wen, X. Jiang, C. Zeng, J. Hong and J. Dai, Modulating the Electrical Transport in the Two-Dimensional Electron Gas at $LaAlO_3/SrTiO_3$ Heterostructures by Interfacial Flexoelectricity, *Phys. Rev. Lett.*, 2019, **122**, 257601.
34 H. Lu, C. W. Bark, D. Esque de los Ojos, J. Alcala, C. B. Eom, G. Catalan and A. Gruverman, Mechanical writing of ferroelectric polarization, *Science*, 2012, **336**, 59–61.
35 J. Narvaez, F. Vasquez-Sancho and G. Catalan, Mechanical writing of ferroelectric polarization, *Nature*, 2016, **538**, 219–221.
36 E. Meirzadeh, D. V. Christensen, E. Makagon, H. Cohen, I. Rosenhek-Goldian, E. H. Morales, A. J. Bhowmik, M. G. Lastra, A. M. Rappe, D. Ehre, M. Lahav, N. Pryds and I. Lubomirsky, Surface Pyroelectricity in Cubic $SrTiO_3$, *Adv. Mater.*, 2019, **31**, 1904733.
37 G. Xu, F. Hao, J. Hong and D. Fang, Atomic-scale simulations for lithium dendrite growth driven by strain gradient, *Appl. Math. Mech. Engl. Ed.*, 2020, **41**, 533–542.
38 K. I. Bolotin, K. Sikes, Z. Jiang, M. Klima, G. Fudenberg, J. Hone, P. Kim and H. Stormer, Ultrahigh electron mobility in suspended graphene, *Solid State Commun.*, 2008, **146**, 351–355.
39 M. D. Stoller, S. Park, Y. Zhu, J. An and R. S. Ruoff, Graphene-based ultracapacitors, *Nano Lett.*, 2008, **8**, 3498–3502.
40 M. Zhou, Y. Zhai and S. Dong, Electrochemical sensing and biosensing platform based on chemically reduced graphene oxide, *Anal. Chem.*, 2009, **81**, 5603–5613.
41 K. S. Kim, Y. Zhao, H. Jang, S. Y. Lee, J. M. Kim, K. S. Kim, J. H. Ahn, P. Kim, J. Y. Choi and B. H. Hong, Large-scale pattern growth of graphene films for stretchable transparent electrodes, *Nature*, 2009, **457**, 706–710.
42 F. Bonaccorso, L. Colombo, G. Yu, M. Stoller, V. Tozzini, A. C. Ferrari, R. S. Ruoff and V. Pellegrini, Graphene related two-dimensional crystals, and hybrid systems for energy conversion and storage, *Science*, 2015, **347**, 1246501.
43 Z. S. Wu, W. Ren, L. Wen, L. Gao, J. Zhao, Z. Chen, G. Zhou, F. Li and H. M. Cheng, Graphene Anchored with Co_3O_4 Nanoparticles as Anode of Lithium Ion Batteries with Enhanced Reversible Capacity and Cyclic Performance, *ACS Nano*, 2010, **4**, 3187–3194.
44 H. Wang, L. F. Cui, Y. Yang, H. S. Casalongue, J. T. Robinson, Y. Liang, Y. Cui and H. Dai, Mn_3O_4–Graphene Hybrid as a High-Capacity Anode Material for Lithium Ion Batteries, *J. Am. Chem. Soc.*, 2010, **132**, 13978–13980.
45 G. Zhou, D. W. Wang, F. Li, L. Zhang, N. Li, Z. S. Wu, L. Wen, G. Q. Lu and H. M. Cheng, Graphene-Wrapped Fe_3O_4 Anode Material with Improved Reversible Capacity and Cyclic Stability for Lithium Ion Batteries, *Chem. Mater.*, 2010, **22**, 5306–5313.
46 C. Uthaisar and V. Barone, Edge effects on the characteristics of Li diffusion in graphene, *Nano Lett.*, 2010, **10**, 2838–2842.
47 Y. Jing, Z. Zhou, C. R. Cabrera and Z. Chen, Metallic VS_2 Monolayer: A Promising 2D Anode Material for Lithium Ion Batteries, *J. Phys. Chem. C*, 2013, **117**, 25409–25413.
48 W. Li, Y. Yang, G. Zhang and Y. W. Zhang, Ultrafast and directional diffusion of lithium in phosphorene for high-performance lithium-ion battery, *Nano Lett.*, 2015, **15**, 1691–1697.
49 K. Persson, V. A. Sethuraman, L. J. Hardwick, Y. Hinuma, Y. S. Meng, A. van der Ven, V. Srinivasan, R. Kostecki and G. Ceder, Lithium diffusion in graphitic carbon, *J. Phys. Chem. Lett.*, 2010, **1**, 1176–1180.
50 K. Toyoura, Y. Koyama, A. Kuwabara, F. Oba and I. Tanaka, First-principles approach to chemical diffusion of lithium atoms in a graphite intercalation compound, *Phys. Rev. B: Condens. Matter Mater. Phys.*, 2008, **78**, 214303.
51 C. Lee, X. D. Wei, J. W. Kysar and J. Hone, Measurement of the Elastic Properties and Intrinsic Strength of Monolayer Graphene, *Science*, 2008, **321**, 385–388.
52 H. Chen, X. L. Zhang, Y. Y. Zhang, D. Wang, D. L. Bao, Y. Que, W. Xiao, S. Du, M. Ouyang, S. T. Pantelides and H. J. Gao, Atomically precise, custom-design origami graphene nanostructures, *Science*, 2019, **365**, 1036–1040.
53 G. Kresse and J. Furthmüller, Efficient iterative schemes for ab initio total-energy calculations using a plane-wave basis set, *Phys. Rev. B: Condens. Matter*, 1996, **54**, 11169–11186.
54 G. Kresse and J. Furthmüller, Efficiency of ab-initio total energy calculations for metals and semiconductors using a plane-wave basis set, *Comput. Mater. Sci.*, 1996, **6**, 15–50.
55 P. E. Blöchl, Projector augmented-wave method, *Phys. Rev. B: Condens. Matter*, 1994, **50**, 17953–17979.
56 J. P. Perdew, J. A. Chevary, S. H. Vosko, K. A. Jackson, M. R. Pederson, D. J. Singh and C. Fiolhais, Atoms Molecules, Solids, and Surfaces: Applications of the Generalized Gradient Approximation for Exchange and Correlation, *Phys. Rev. B: Condens. Matter*, 1992, **46**, 6671–6687.
57 S. Grimme, Semiempirical GGA-type density functional constructed with a long-range dispersion correction, *J. Comput. Chem.*, 2006, **27**, 1787–1799.
58 G. Henkelman, B. P. Uberuaga and H. Jónsson, A climbing image nudged elastic band method for finding saddle points and minimum energy paths, *J. Chem. Phys.*, 2000, **113**, 9901–9904.
59 G. Henkelman and H. Jónsson, Improved tangent estimate in the nudged elastic band method for finding minimum energy paths and saddle points, *J. Chem. Phys.*, 2000, **113**, 9978–9985.
60 S. Nosé, A unified formulation of the constant temperature molecular dynamics methods, *J. Chem. Phys.*, 1984, **81**, 511–519.

61 I. V. Lebedeva, A. A. Knizhnik, A. M. Popov, Y. E. Lozovik and B. V. Potapkin, Interlayer interaction and relative vibrations of bilayer graphene, *Phys. Chem. Chem. Phys.*, 2011, **13**, 5687–5695.
62 J. H. Wong, B. R. Wu and M. F. Lin, Strain effect on the electronic properties of single layer and bilayer graphene, *J. Phys. Chem. C*, 2012, **116**, 8271–8277.
63 Y. X. Zhao and I. L. Spain, X-ray diffraction data for graphite to 20 GPa, *Phys. Rev. B: Condens. Matter Mater. Phys.*, 1989, **40**, 993–997.
64 X. Fan, W. T. Zheng and J. L. Kuo, Adsorption and diffusion of Li on pristine and defective graphene, *ACS Appl. Mater. Interfaces*, 2012, **4**, 2432–2438.
65 J. Hong, G. Catalan, J. F. Scott and E. Artacho, The flexoelectricity of barium and strontium titanates from first principles, *J. Phys.: Condens. Matter*, 2010, **22**, 112201–112206.
66 F. Hao, D. Fang and X. Chen, The coupling of strain and lithium diffusion: a theoretical model based on first-principles calculations, *J. Electrochem. Soc.*, 2015, **162**, A2266–A2270.
67 K. J. Laidler, *Chemical Kinetics*, McGraw-Hill, New York, 1965, vol. 15.
68 M. Becton and X. Wang, Thermal gradients on graphene to drive nanoflake motion, *J. Chem. Theory Comput.*, 2014, **10**, 722–730.
69 S. C. Hernández, C. J. C. Bennett, C. E. Junkermeier, S. D. Tsoi, F. J. Bezares, R. Stine, J. T. Robinson, E. H. Lock, D. R. Boris, B. D. Pate, J. D. Caldwell, T. L. Reinecke, P. E. Sheehan and S. G. Walton, Chemical gradients on graphene to drive droplet motion, *ACS Nano*, 2013, **7**, 4746–4755.
70 P. Kovaříček, M. Cebecauer, J. Neburková, J. Bartoň, M. Fridrichová, K. A. Drogowska, P. Cigler, J. M. Lehn and M. Kalbac, Proton-Gradient-Driven Oriented Motion of Nanodiamonds Grafted to Graphene by Dynamic Covalent Bonds, *ACS Nano*, 2018, **12**, 7141–7147.